NBSIR 75-703

A Failure Hypothesis for Masonry Shearwalls

Felix Y. Yokel and S. George Fattal

Center for Building Technology
Institute for Applied Technology
National Bureau of Standards
Washington, D. C. 20234

May 1975

Final Report

Prepared for

Cooperative Masonry Project:

Center for Building Technology
Brick Institute of America
Masonry Institute of America
National Concrete Masonry Association
Tri-Service Building Materials Investigational Program

NBSIR 75-703

A FAILURE HYPOTHESIS FOR MASONRY SHEARWALLS

Felix Y. Yokel and S. George Fattal

Center for Building Technology
Institute for Applied Technology
National Bureau of Standards
Washington, D. C. 20234

May 1975

Final Report

Prepared for

Cooperative Masonry Project:
Center for Building Technology
Brick Institute of America
Masonry Institute of America
National Concrete Masonry Association
Tri-Service Building Materials Investigational Program

U.S. DEPARTMENT OF COMMERCE, Rogers C.B. Morton, *Secretary*
James A. Baker, III, *Under Secretary*
Dr. Betsy Ancker-Johnson, *Assistant Secretary for Science and Technology*

NATIONAL BUREAU OF STANDARDS, Ernest Ambler, *Acting Director*

Table of Contents

List of Figures:

List of Symbols

The following symbols are used in this paper:

b width of panel

f'_m unconfined compressive strength of masonry

f''_s calculated strength parameter defined as the apparent splitting strength if $\sigma_3 = 0$.

f'_t flexural tensile strength of horizontal masonry cross section

P_d diagonal compressive load

P'_d diagonal load capacity when $P_v = 0$

P_v resultant vertical edge load

R' ratio $f'_m/\bar{\tau}'_d$

R ratio f'_m/f''_s

t thickness of panel

α angle of σ_3 with horizontal

β_p unconfined compressive strength of concrete

σ_v P_v/bt

μ coefficient in the joint separation equation

ν Poisson's Ratio

σ_1 principal tensile (or smaller compressive) stress in-plane of panel

σ_3 principal compressive stress in plane of panel

σ_2 principal stress normal to plane of panel

$\bar{\sigma}_y$ nominal vertical stress (perpendicular to bed joints)

$\bar{\tau}$ nominal shear stress (parallel to bed joints)

$\bar{\tau}'_d = \dfrac{0.707\ P'_d}{bt}$ nominal shear strength when $P_v = 0$

$\bar{\tau}''_d$ calculated strength parameter

$\bar{\tau}_o$ shear strength at $\bar{\sigma}_y = 0$

$\bar{\tau}''_o$ calculated strength parameter in an approximate equation for in-plane splitting failure

Subscript "c" denoting "critical," identifies stress at failure.

"Prime" as in f'_m or $\bar{\tau}'_d$ denotes a measured strength term.

"Double prime" such as in f''_s denotes a calculated strength parameter

A FAILURE HYPOTHESIS FOR MASONRY SHEAR WALLS*

by

Felix Y. Yokel and S. George Fattal

Various failure hypotheses for wall panels subjected simultaneously to diagonal compressive load and to vertical compressive edgeload are compared with the results of thirty two tests on four types of brick masonry walls which were published elsewhere. It is concluded that failure can occur by joint separation or by splitting. A failure hypothesis is advanced which is shown to be in good agreement with the test results examined.

Key Words: Brick; failure; failure theories; masonry; shear walls; shear strength; shear test; stresses; stress distribution; structural engineering.

1. Introduction

This study deals with the load capacity of clay masonry walls subjected to a diagonal compressive load combined with a compressive edge load acting in the plane of the wall and normal to the direction of the mortar bed joints. The loading and boundary conditions of these walls are similar to those encountered in certain shear wall elements in buildings.

2. Scope

Various failure hypotheses are compared with the results of thirty-two tests of 48 in. x 48 in. (122 cm. x 122 cm.) single-wythe clay-brick walls which were published elsewhere [4][1/]. A failure hypothesis is advanced which accounts for the observed failure modes.

3. Loading Condition

The loading condition studied is shown in figure 1. P_d is the diagonal compressive load and P_v is the resultant of the distributed edge load. For the purpose of this study, the following nominal stresses are introduced: $\bar{\tau}$, the

1/ Numbers in brackets refer to literature references in Appendix I.

*Research performed by the Cooperative Masonry Project: Center for Building Technology, Brick Institute of America, Masonry Institute of America, National Concrete Masonry Association, Tri-Service Building Materials Investigational Program Committee.

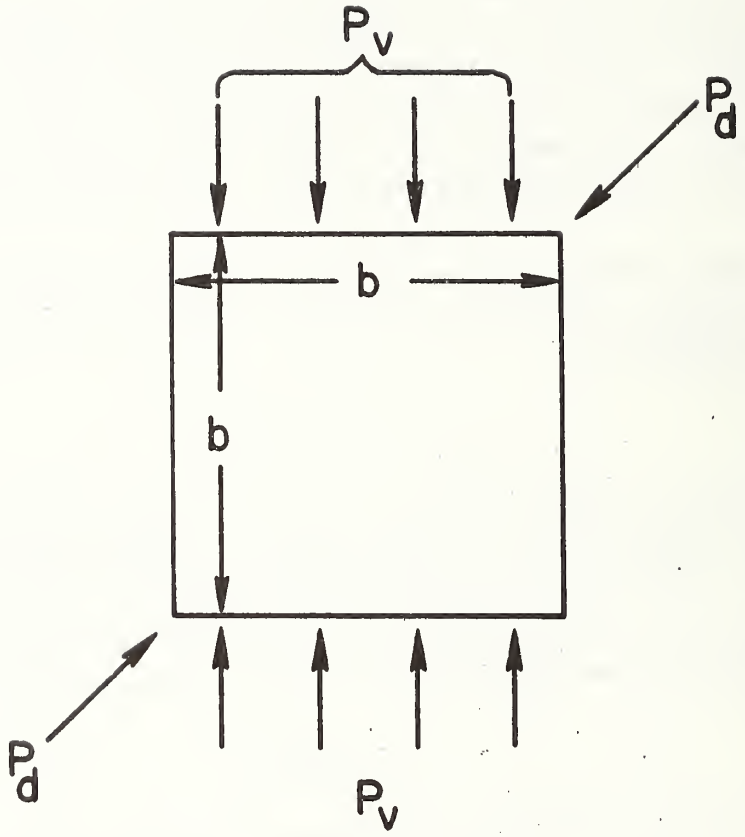

FIGURE 1 LOADING CONDITION

nominal shear stress, is the horizontal component of P_d divided by the horizontal cross sectional area, bt; $\bar{\sigma}_y$, the nominal vertical stress, is the resultant vertical component of the applied load which consists of P_v and the vertical component of P_d, divided by the horizontal cross sectional area. In the actual tests examined in this report wall width, b, was approximately 48 in. (122 cm) and wall thickness, t, was approximately 3.7 in. (9.4 cm.). Load P_d was transmitted by a triangular loading shoe with a 6 in. (15 cm) side length and P_v was transmitted by three 11 in. (28 cm)long loading blocks.

4. Stress Distribution

In this analysis it is assumed that strength can be correlated with hypothetical stress levels at failure, calculated using an isotropic linearly-elastic model. In view of the lack of specific information on the directional variation of the elastic properties of the test specimens an anisotropic model was not feasible. However, a numerical analysis using a 2 to 1 ratio between the orthogonal elastic moduli indicated that the results of the analysis presented in this study will not be significantly altered by considerations of orthotropy. Actual local stresses resulting from discontinuities and material flaws are likely to differ from the calculated stresses.

The elastic stress distribution on a square plate loaded by P_d alone was approximately calculated by Frocht [3] who also documented reasonable agreement between calculated stresses and those observed in a photoelastic model. Frocht simplified his equations by assuming Poisson's Ratio to be zero.

In figure 2, Frocht's solution is compared with the results of a finite element analysis using 78 elements in the first quadrant (y = 0 to h, x = 0 to h), with element sizes of h/16 near the center and the corners and h/8 elsewhere. The calculated stress distribution is shown for $\nu = 0$ and $\nu = 0.3$, in which ν is Poisson's Ratio. For the case $\nu = 0$ the principal tensile stress in the center of the panel calculated by the finite element method was 4 percent less, and the principal compressive stress 3 percent more than the corresponding stresses calculated by Frocht. For the case $\nu = 0.3$, the tensile stress calculated by the finite element method approximately equaled Frocht's solution and the compressive stress was 4 percent less. On the basis of the finite element investigation it was concluded that the effect of Poisson's ratio on the magnitude and distribution of calculated stresses is not significant enough to warrant consideration in this study.

In figure 2, principal stresses are shown non-dimensionally as multiples of $\bar{\tau}$. In the following discussion σ_1 always denotes the principal tensile stress or the smaller principal compressive stress in the plane of the

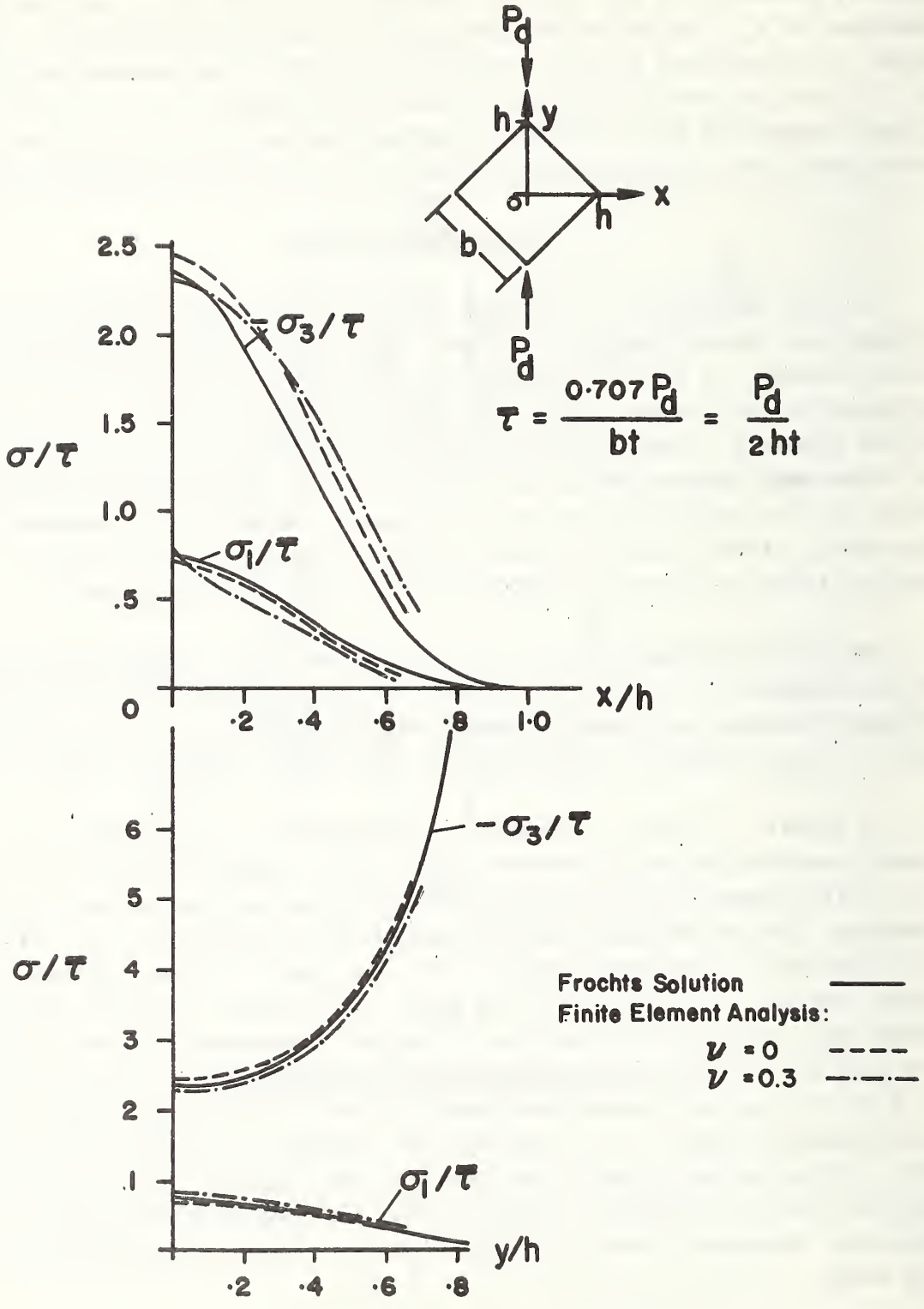

FIGURE 2 STRESS DISTRIBUTION

wall, σ_3 denotes the (larger) principal compressive stress in the plane of the wall and σ_2, the principal stress normal to the plane of the wall, is assumed 0.

Frocht calculated the following principal stresses in the center of the wall in figure 2:

$$\sigma_1 = 0.7336\bar{\tau} \qquad \ldots\ldots (1)$$

$$\sigma_3 = -2.380\bar{\tau} \qquad \ldots\ldots (2)$$

in which compressive stresses are negative, tensile stresses are positive, and $\bar{\tau}$ is assumed positive. A Mohr Circle representation of the corresponding state of stress is shown in figure 3(a), which also shows the stesses on an infinitesimal cube whose sides are parallel to the sides of the wall. The orientation of the plane normal to σ_1 with respect to the horizontal (the direction of bed joints is assumed "horizontal") is at an angle $\alpha = 45°$.

Figure 3(b) shows the state of stress calculated in the center of a panel subjected simultaneously to P_d and P_v. Superposition is used by adding stress $\sigma_v = \frac{P_v}{bt}$ to the stresses acting on the infinitesimal cube shown in figure 3. The following expressions can be derived from Mohr's Circle shown in figure 3(b):

$$\sigma_1 = -0.823\bar{\tau} + \frac{\sigma_v}{2} + \sqrt{(1.556\bar{\tau})^2 + \frac{\sigma_v^2}{4}} \qquad \ldots\ldots (3)$$

$$\sigma_3 = -0.823\bar{\tau} + \frac{\sigma_v}{2} - \sqrt{(1.556\tau)^2 + \frac{\sigma_4^2}{4}} \qquad \ldots\ldots (4)$$

$$\alpha = \frac{1}{2}\ cot^{-1}\left(\frac{\sigma_v}{3.112\tau}\right) \qquad \ldots\ldots (5)$$

in these expressions σ_v is negative if P_v is compressive and positive if P_v is tensile. $\bar{\tau}$ is always assumed positive.

5. Failure Hypotheses

5.1 General

Not all the failure hypotheses that have been advanced for materials similar to masonry are investigated in detail, since the test information considered does not provide an adequate basis for such an approach. Three failure hypotheses for splitting and one hypothesis for joint separation are considered.

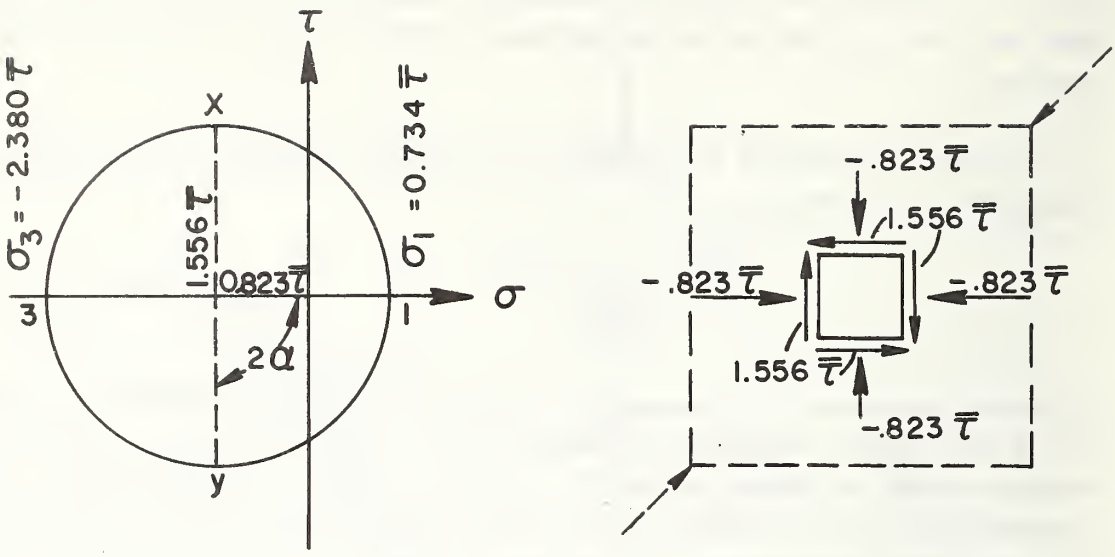

(a) PANEL LOADED BY P_d ALONE

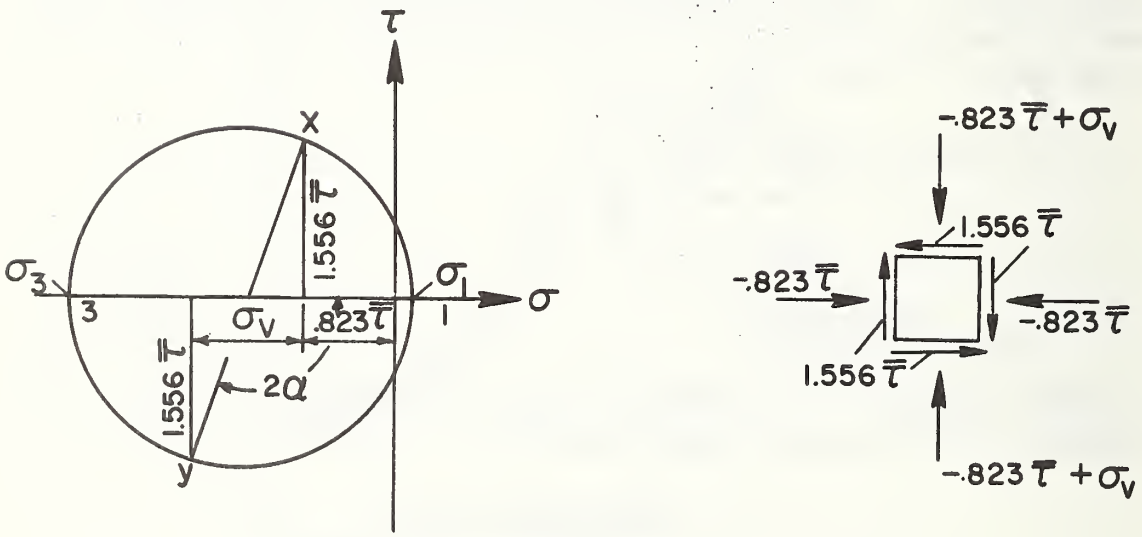

(b) PANEL LOADED BY P_d and P_V

FIGURE 3 CALCULATED STATE OF STRESS IN THE CENTER OF A PANEL

The hypotheses for splitting are: failure by critical normal stress; failure by a critical biaxial combination of normal principal stresses, a concept, recently corroborated for concrete by test results [8], which covers a broad spectrum of different failure hypotheses advanced in the past; failure at a critical in-plane tensile (extensional) strain, a hypothesis which could be utilized in a single failure criterion which would account for "tensile", as well as "compressive" failures.

Failures that are actually documented for the tests discussed in this paper are shown in figures 4 through 6 and can be placed in three general categories:

1. Separation along mortar joints. (See, for instance, figure 4., Specimen AC2)
2. Splitting, generally in the direction of σ_1 (the "direction of splitting" is taken as the direction in which material particles separate, which is normal to the direction of crack propagation), in a region along the loaded diagonal which includes the center of the panel. (See, for instance, figure 5, AH2-4)
3. Splitting, approximately in the direction of σ_1, most severe in the vicinity of the loading fixtures and not necessarily including the center of the panel. (See, for instance, figure 5, AH8),

No evidence of failures by crushing of masonry units or mortar joints or by splitting in the direction normal to the plane of the wall is observed in the records available.

The following investigation of failure hypotheses related to splitting is entirely based on the elastic state of stress in the center of the panel. This approach provides a valid predictive model if two conditions are satisfied:

1. The failure is brittle (there is no substantial re-distribution of stresses at load levels lower than those defined as failure loads).
2. The most critical condition occurs at or near the center of the panel.

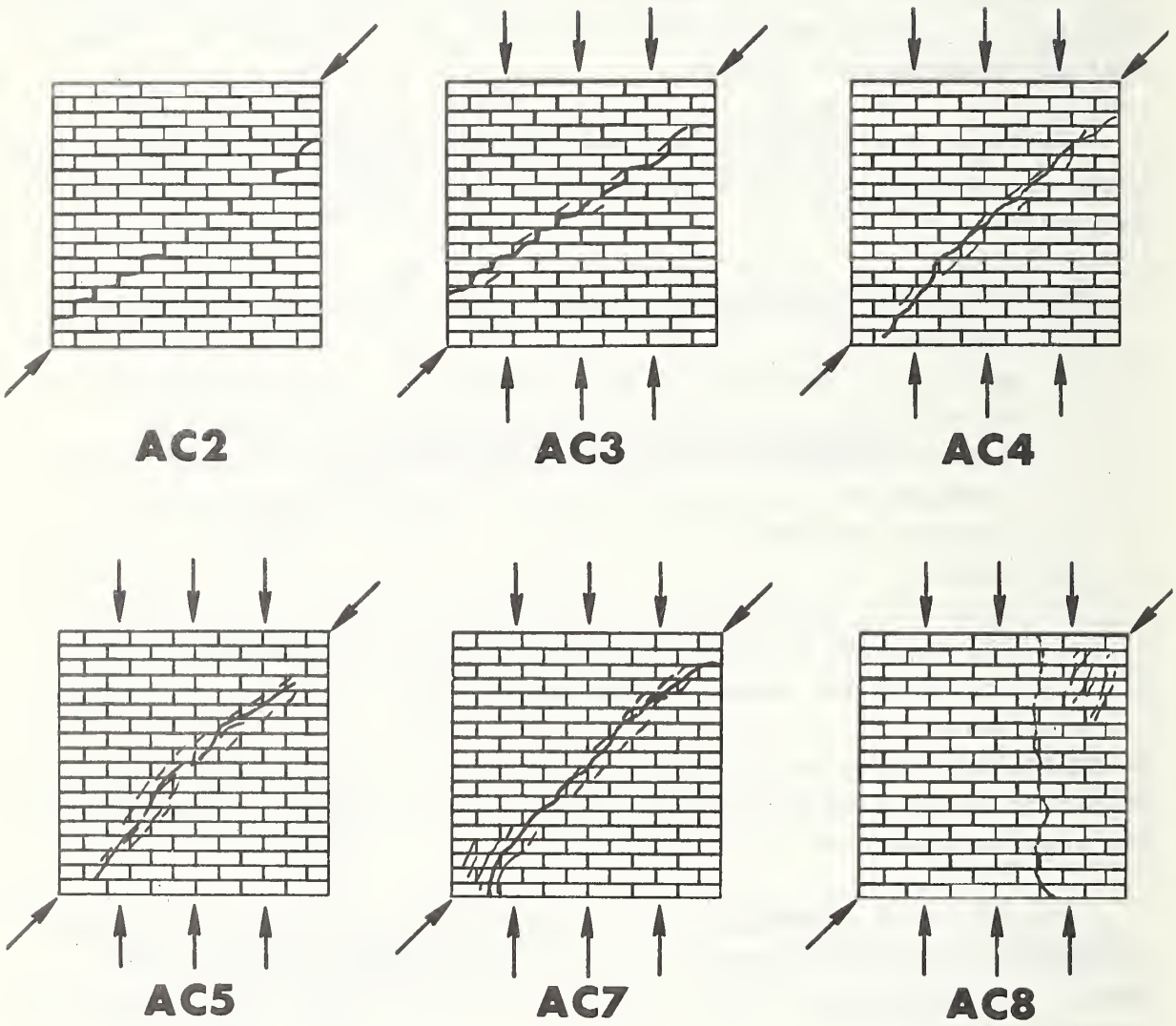

FIGURE 4 FAILURE MODES OF SPECIMENS TYPE AC

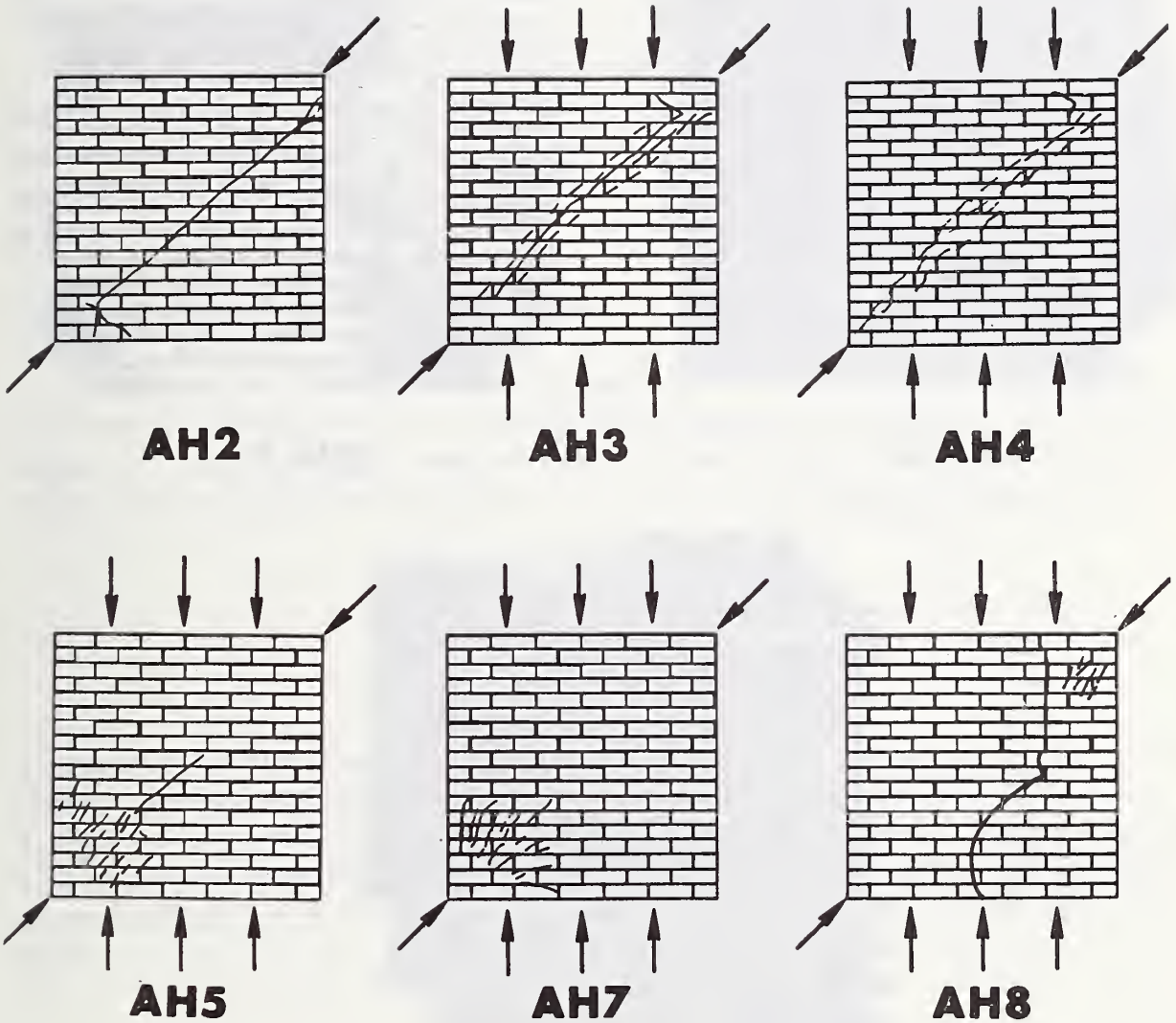

FIGURE 5 FAILURE MODES OF SPECIMENS TYPE AH

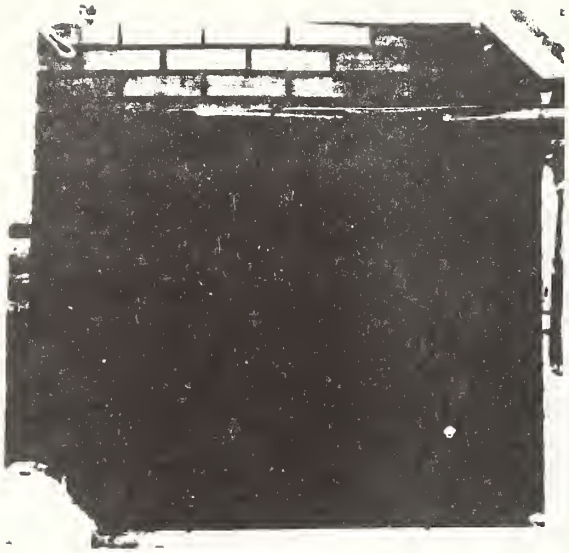

BH 3

BH 7

SH 5

FIGURE 6 FAILURE MODES OF SPECIMENS TYPE BH AND SH

For splitting failures (categories 2 and 3) the first condition is reasonably satisfied. The second condition is satisfied for failure category 2 previously discussed in this section, but not necessarily for failure category 3 where the most critical conditions may occur in locations other than the center of the panel.

The interpretation of compression failures near the corner fixtures and the loading blocks would have to account for the complex confining effect of these devices. This was not attempted since the load transfer conditions causing category 3 failures in test specimens are not normally anticipated in shearwall elements of buildings.

5.2 Failure by Critical Normal Stress

According to this hypothesis the wall would fail either if σ_1 exceeds the tensile strength or if σ_3 exceeds the compressive strength. Curve 1 in figure 7[2/] shows critical combinations of $\bar{\tau}$ and $\bar{\sigma}_y$ that would cause failure in accordance with this hypothesis. $\bar{\tau}$ and $\bar{\sigma}_y$ are given as multiples of

$$\bar{\tau}'_d = \frac{0.707\ P'_d}{bt} \qquad \ldots\ (6)$$

in which P'_d is the diagonal failure load when $P_v = 0$ ($\bar{\tau}/\tau'_d = 1$, $\bar{\sigma}_y/\tau'_d = -1$). Curve 1 was calculated on the basis of the premise that at $\bar{\tau}/\bar{\tau}'_d = 1$, and $\bar{\sigma}_y/\bar{\tau}'_d = -1$, σ_1 equaled the tensile strength of the material. Curves 1(a) and 1(b) represent compressive failures in the center of the panel corresponding to two ratios: $R' = -8.3$, and $R' = -9.7$ typical for the test specimens in which

$$R' = \frac{f'_m}{\bar{\tau}'_d} \qquad \ldots\ (7)$$

and f'_m is the (unconfined) compressive strength. As previously noted, in the specific tests examined, compressive failure apparently did not originate in the center of the panel. The information conveyed by curves 1(a) and 1(b) is therefore not applicable to the test results.

Curve 1 was calculated without specific consideration of directional variations in splitting strength. Such variations are known to exist. Johnson and Thompson [6] reported an increase in splitting strength as the

---

[2/] The equations for all the failure envelopes shown in figure 7 are derived in the appendix.

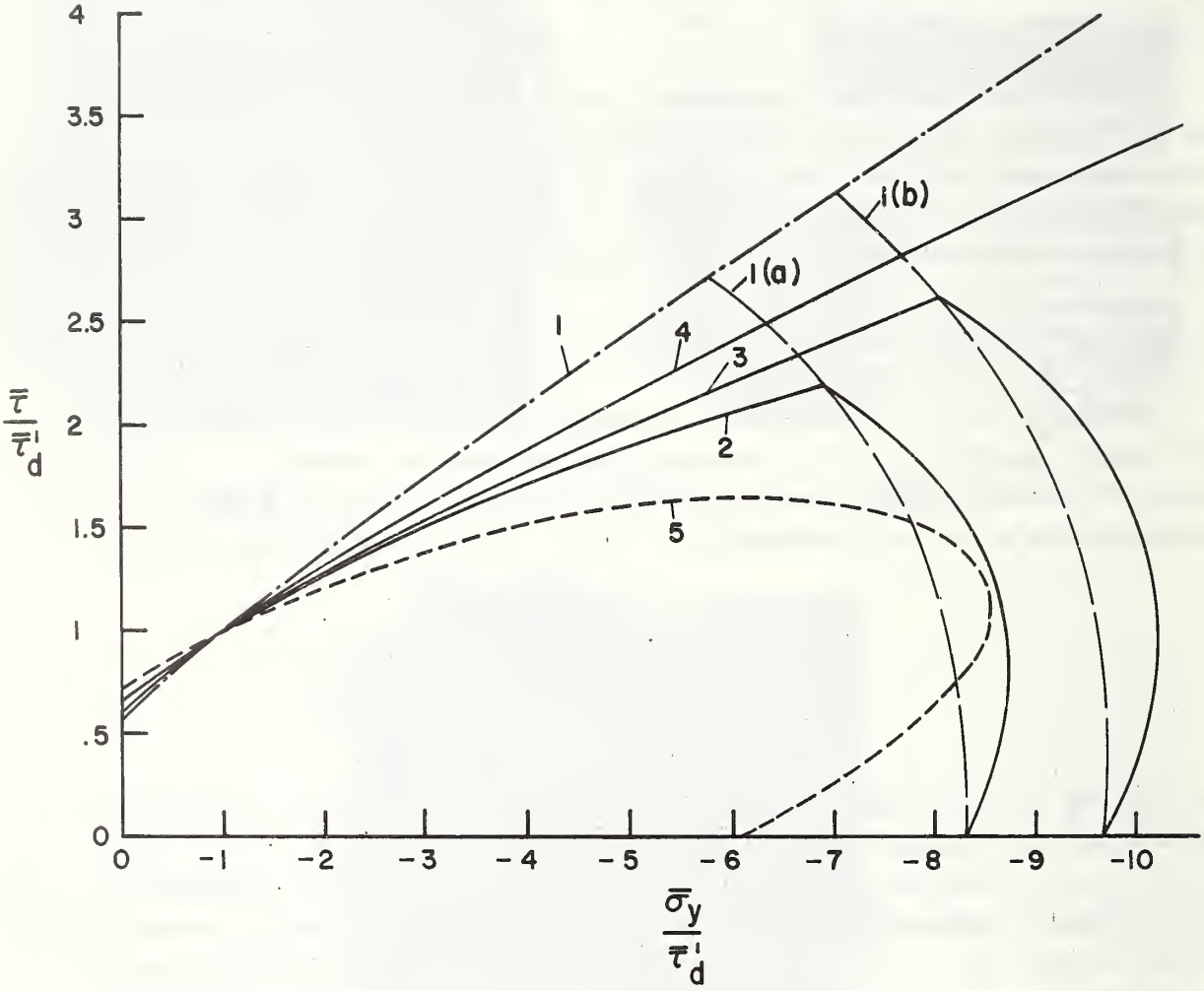

FIGURE 7 FAILURE HYPOTHESES FOR SPLITTING

orientation of the splitting crack with respect to the horizontal (direction of bed joints), (α), increases from 0° to 90°. For a change from 45° to 90°, the range occuring between $\bar{\sigma}_y/\bar{\tau}'_d = -1$ and $\bar{\sigma}_y/\bar{\tau}'_d = f'_m/\bar{\tau}'_d$, the reported strength increase ranged from 6 percent for masonry with a 90°-splitting strength of 490 psi (3.38 MPa) to 25 percent for masonry with a 90°-splitting strength of 275 psi (1.9 MPa). Consideration of such a change in strength would increase the calculated strength when $\bar{\sigma}_y/\bar{\tau}'_d < -1$. The calculated strength when $\bar{\sigma}_y/\bar{\tau}'_d > -1$ would decrease considerably if the substantial decrease in splitting strength from $\alpha = 45°$ to $\alpha = 0°$ were considered. This range is not examined in this paper, since no pertinent test results are available.

5.3 Failure by a Critical Combination of Normal Principal Stresses

This hypothesis assumes that both principal stresses in the plane of the wall contribute to the failure as suggested by Griffith for brittle fracture [5]. Recent experimental work by Kupfer et al. [8] corroborates this concept for concrete. One of Kupfer's strength envelopes for concrete is shown in figure 8(a). A strength envelope determined by Khoo and Hendry [7] from biaxial tests on 1 in.-square by 3 in. (2.5 cm-square x 7.6 cm) specimens cut from 1/3-scale model brick is shown in figure 8(b). Khoo's interaction curve does not reflect the effect of the mortar in the brick masonry since the specimens were cut from a brick unit. The assumed strength envelope for masonry used in this investigation is shown in figure 8(c). In the range $\sigma_3 \leq 0 \leq \sigma_1$, the simplified linear strength envelope in the second quadrant of figure 8(c) satisfies "Mohr's Failure Theory" [12], and is uniquely defined by two points: one corresponding to the state of stress at failure under vertical compressive load, $\sigma_1 = 0$, $\sigma_3 = f'_m$; and the other corresponding to the previously-defined state of stress under failure load P'_d, $\sigma_1 = 0.7336\ \bar{\tau}'_d$, $\sigma_3 = -2.380\ \bar{\tau}'_d$. Parameter f''_s, the apparent major principal stress at failure when $\sigma_3 = 0$, is derived as:

$$f''_s = 0.7336\ \bar{\tau}'_d \frac{f'_m}{(f'_m + 2.38\ \bar{\tau}'_d)} \qquad \ldots\ldots (8)$$

The nondimensional parameter R defined by

$$R = \frac{f'_m}{f''_s} \qquad \ldots\ldots (9)$$

and introduced in figure 8(c) for convenience, is related to the measured quantity $R' = \frac{f'_m}{\bar{\tau}'_d}$ by the following equation:

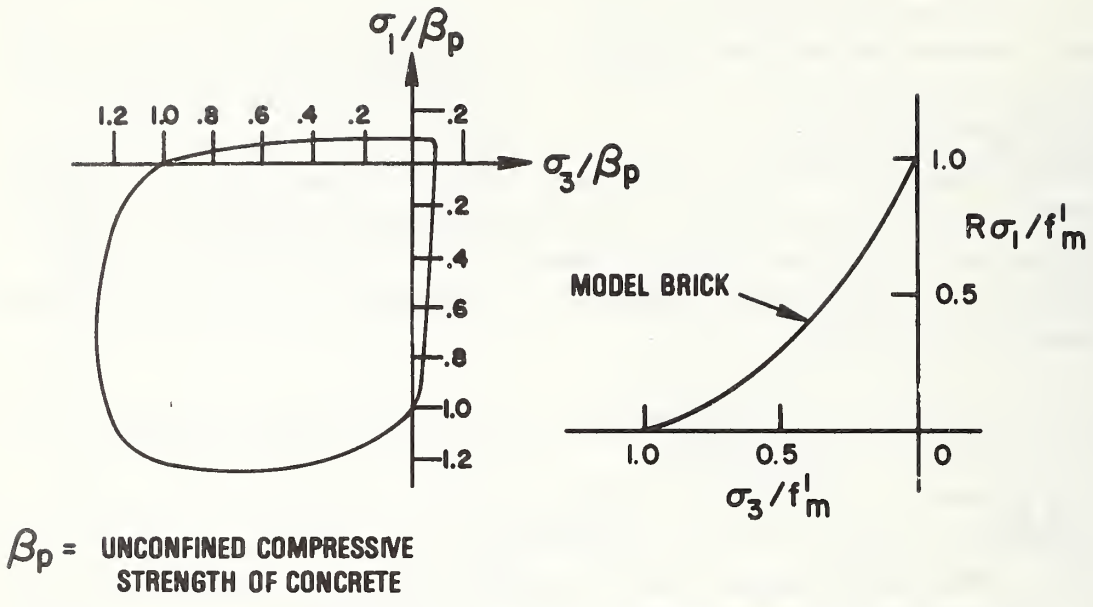

(a) CONCRETE (KUPFER et AL.)

(b) MODEL BRICK (KHOO & HENDRY)

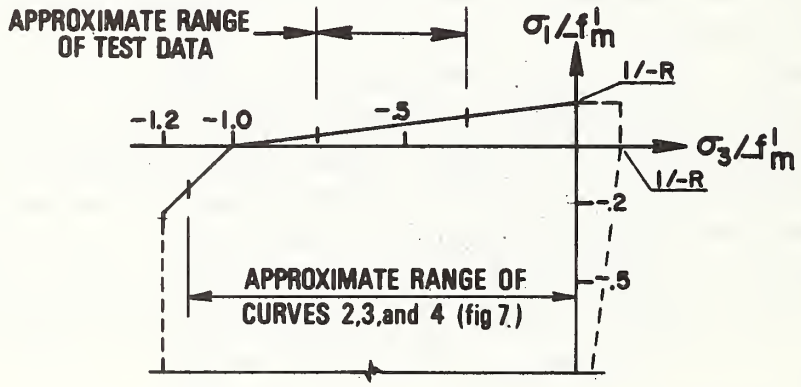

(c) ASSUMED STRENGTH ENVELOPE

FIGURE 8 STRENGTH ENVELOPES

$$R = 1.36\ R' + 3.24 \qquad \ldots\ldots (10)$$

In accordance with the strength envelope in figure 8(c) failure would occur at the following critical stresses:

if $\sigma_3 \leq 0 \leq \sigma_1$

$$\sigma_1 = f''_s - \frac{\sigma_3}{R} = \frac{f'_m - \sigma_3}{R} \qquad \ldots\ldots (11)$$

if $\sigma_1 = 0$

$$\sigma_3 = f'_m \qquad \ldots\ldots (12)$$

if $\sigma_1 < 0$

$$\sigma_3 = f'_m + \sigma_1 \geq 1.2\ f'_m \qquad \ldots\ldots (13)$$

In eq. (11) σ_1 is positive, in eq. (13) σ_1 is negative, and σ_3, f'_m and ratio R are negative.

The data in figure 8 indicate that the interaction curve between point $\sigma_3 = f'_m$, $\sigma_1 = 0$ and point $\sigma_3 = 0$, $\sigma_1 = f'_m/R$ may not necessarily be linear. It is also know that the splitting strength changes with the orientation of σ_1, and tends to decrease substantially as σ_1 becomes normal to the mortar bed joints [6]. It is assumed that for the loading and boundary conditions considered in this study, figure 8(c) which is used to derive equations (11) through (13) should lead to an approximate estimate of strength in the range $\bar{\sigma}_y/\bar{\tau}'_d \leq -1$. When extrapolated to the range $\bar{\sigma}_y/\bar{\tau}'_d > -1$ which corresponds to a tensile edge load P_v, for which no test data are available, the estimate is probably too high, with the discrepancy increasing as $\alpha \to 0$. For more general application of this hypothesis the directional variation in the splitting strength would have to be considered, so that:

$$\text{at failure } \sigma_1 = f(\sigma_3, \alpha) \qquad \ldots\ldots (14)$$

In figure 7 the interaction curves, calculated by this failure hypothesis, are shown as curves 2, 3, and 4 for values of R = -8, R = -10, and R = -16, respectively. The previously discussed qualifications for compressive failure also apply to the descending part of these curves, which signify "compressive failures." As in previous cases, calculated nominal stresses at failure are based on the premise, that at $\bar{\sigma}_y/\bar{\tau}'_d = -1$, and $\bar{\tau}/\bar{\tau}'_d = 1$, failure occurs by the failure criteria of this hypothesis. As previously noted, the extension of the curves to $\bar{\sigma}_y/\bar{\tau}'_d > -1$ probably overestimates strength.

5.4 Failure by Critical Tensile (Extensional) Strain

In accordance with this hypothesis failure occurs when a critical tensile strain is exceeded:

$$\sigma_1 - \nu\sigma_3 = \text{constant} \qquad \ldots\ldots (15)$$

In this case Poisson's Ratio (ν) has a considerable effect on calculated load capacity. Not much information is available on Poisson's Ratio for clay masonry. For concrete a range from 0.16 to 0.25 was reported [9]. Blume et al. [2] estimated Poisson's Ratio of reinforced brick masonry used in their test program to range from 0.10 to as much as 0.25 at high stresses, and Sahlin [10] reports measurements ranging from 0.2 at initial loading to 0.35 at ultimate load on 3 x 3 x 6 cm prisms cut from brick units. For this study a ratio of 0.2 was assumed. Curve 5 in figure 7 was calculated, assuming that, at failure:

$$\sigma_1 - 0.2\,\sigma_3 = \text{constant.} \qquad \ldots\ldots (16)$$

As for the previous failure hypotheses, curve 5 is normalized so that failure would occur at $\bar{\tau}/\bar{\tau}'_d = 1$, $\sigma_y/\bar{\tau}'_d = -1$. It can be seen from curve 5 that, by this hypothesis, failure under edge load P_v alone would occur at $\sigma_y/\bar{\tau}'_d = -6.05$. However P_v could be increased if a diagonal load is simultaneously applied. This apparent strength increase can be explained by the fact that, within certain limits, principal extensional strains decrease when diagonal load P_d is superposed on edge load P_v.

It is noted that in the range $\sigma_3 \leq 0 \leq \sigma_1$ the critical tensile strain hypothesis is identical to the strength envelope in figure 8(c) if $\nu = -\frac{1}{R}$. For the three typical values observed for the specimens examined herein of R = -8, R = -10 and R = -16, the corresponding ν values would be 0.125, 0.1 and 0.063. These ratios appear to be low when compared with available information, even though that information is very limited.

5.5 Failure by Joint Separation

A typical joint separation failure is shown in figure 4 for specimen AC2. A criterion for joint separation, reported by many investigators [11], can be formulated as follows:

$$\bar{\tau}_c = \bar{\tau}_o - \mu\bar{\sigma}_y \qquad \ldots\ldots (17)$$

in which $\bar{\tau}_c$ is the nominal shear stress at failure,

$\bar{\tau}_o$ is the nominal shear stress at failure when $\bar{\sigma}_y = 0$, and μ is a coefficient, viewed by some authors to be attributable to friction [11].

Since this criterion is stated in terms of nominal stresses it can be postulated that the failure load is not sensitive to the stress distribution producing the nominal stresses as long as a change in stress distribution does not precipitate a change in the failure mode.

6. Analysis of the Test Results

6.1 Test Data

The test data taken from reference [4] are summarized in Tables 1, 2, and 3. Three brick types and two mortar types were used. Table 1 shows the properties of the brick units which were measured in accordance with ASTM C67 [1]. The brick were used to produce four types of masonry designated AC, AH, BH, and SH, in which the first letter designates the type of brick used and the second letter the type of mortar. "C" stands for conventional mortar, "H" stands for high-bond mortar which had a polyvinylidene chloride admixture to increase the flexural strength of the masonry.

Table 2 gives the measured unconfined compressive, and flexural tensile strengths of a horizontal cross section for each type of masonry.

The test results are summarized in Table 3. In columns 7 and 8 of the table nominal failure stresses are given as multiples of the average value of $\bar{\tau}'_d$. Specimens AC1, AC2, and AC3 failed by joint separation (see figure 4) and it is reasoned that $\bar{\tau}'_d$ would therefore not be a meaningful measure of splitting strength. A parameter $\bar{\tau}''_d$ was therefore calculated, using specimen AC4 which was arbitrarily selected, being the specimen with the lowest vertical edge load which gives no visual indication of joint separation failure, and the strength envelope in figure 3(c) with an R value of -16. $\bar{\tau}''_d$ was calculated to be approximately 1.3 $\bar{\tau}'_d$.

6.2 Comparison of the Test Results with Load Capacities Predicted by the Failure Hypotheses.

6.2.1 Masonry Type AC

Figure 9 shows a plot of Test Series AC together with curves 1, 4, and 5 for the three failure hypotheses for splitting (refer also to figure 7). The failure modes of the Type AC specimens are shown in figure 4. As previously noted, specimens AC1, AC2, and AC3 definitely failed by joint separation. A straight line connecting AC3 with the average of AC1 and AC2 is approximated by the equation:

Table 1. Brick Units

Designation	Unit Compressive Strength in psi	Modulus of Rupture in psi	Initial Rate of Absorption g/ (min. x 30 $in.^2$)	Type of Unit
A	14.480	848	6.2	cored
B	20,660	761	2.6	cored
C	17,560	741	19.8	solid

Note: 1 psi = 6.9 kPa 1 $in.^2$ = 6.45 $cm.^2$

Table 2. Masonry Properties (based on gross area)

Type	Compressive Strength f'_m in psi	Flexural Strength f'_t in psi
AC	-3,190	80
AH	-4,830	360
BH	-5,170	452
SH	-6,100	220

Note: 1 psi = 6.9 Pa

Table 3. Test Results

Type	Specimen	P_v in kip	P_d in kip	$-\bar{\sigma}_y$ in psi	$\bar{\tau}$ in psi	$-\frac{\bar{\sigma}_y}{\bar{\tau}'_d}$	$\frac{\bar{\tau}}{\bar{\tau}'_d}$
	AC1	0	44	175	175	.753[a]	.753[a]
	AC2	0	45.5	181	181	.780	.780
	AC3	25	68	410	270	1.766	1.162
	AC4	50	89.2	636	355	2.739	1.529
AC	AC5	75	115	878	457	3.782	1.968
	AC6	100	127	1068	506	4.600	2.179
	AC7	125	133	1232	530	5.306	2.283
	AC8	150	141	1409	560	6.073	2.412
	AH1	0	141	560	560	1.101	1.101
	AH2	0	115	457	457	0.898	0.898
	AH3	50	168.5	951	670	1.870	1.318
	AH4	100	178	1270	708	2.498	1.392
AH	AH5	150	238	1778	946	3.497	1.860
	AH6	200	209.5	1953	833	3.841	1.638
	AH7	250	258	2420	1020	4.759	2.006
	AH8	450	233	3456	926	6.796	1.821
	BH1	0	161	608	608	0.973	.973
	BH2	0	167.5	642	642	1.027	1.027
	BH3	50	245	1191	924	1.906	1.478
	BH4	50	231	1139	872	1.822	1.395
BH	BH5	100	205	1308	774	2.093	1.238
	BH6	100	246	1728	928	2.765	1.485
	BH7	200	261	2050	984	3.280	1.574
	BH8	300	280	2651	1056	4.242	1.690
	SH1	0	167	690	690	.932	.932
	SH2	0	175	724	724	.978	.978
	SH3	0	195	806	806	1.089	1.089
	SH4	50	217	1191	898	1.609	1.214
SH	SH5	100	257	1646	1060	2.224	1.432
	SH6	125	274	1862	1130	2.516	1.527
	SH7	150	297	2109	1230	2.850	1.662
	SH8	200	306	2452	1280	3.313	1.730

Note: 1 kip = 4.45 kN 1 psi = 6.9 kPa

[a] In AC specimens $\bar{\tau}''_d$ is substituted for $\bar{\tau}'_d$

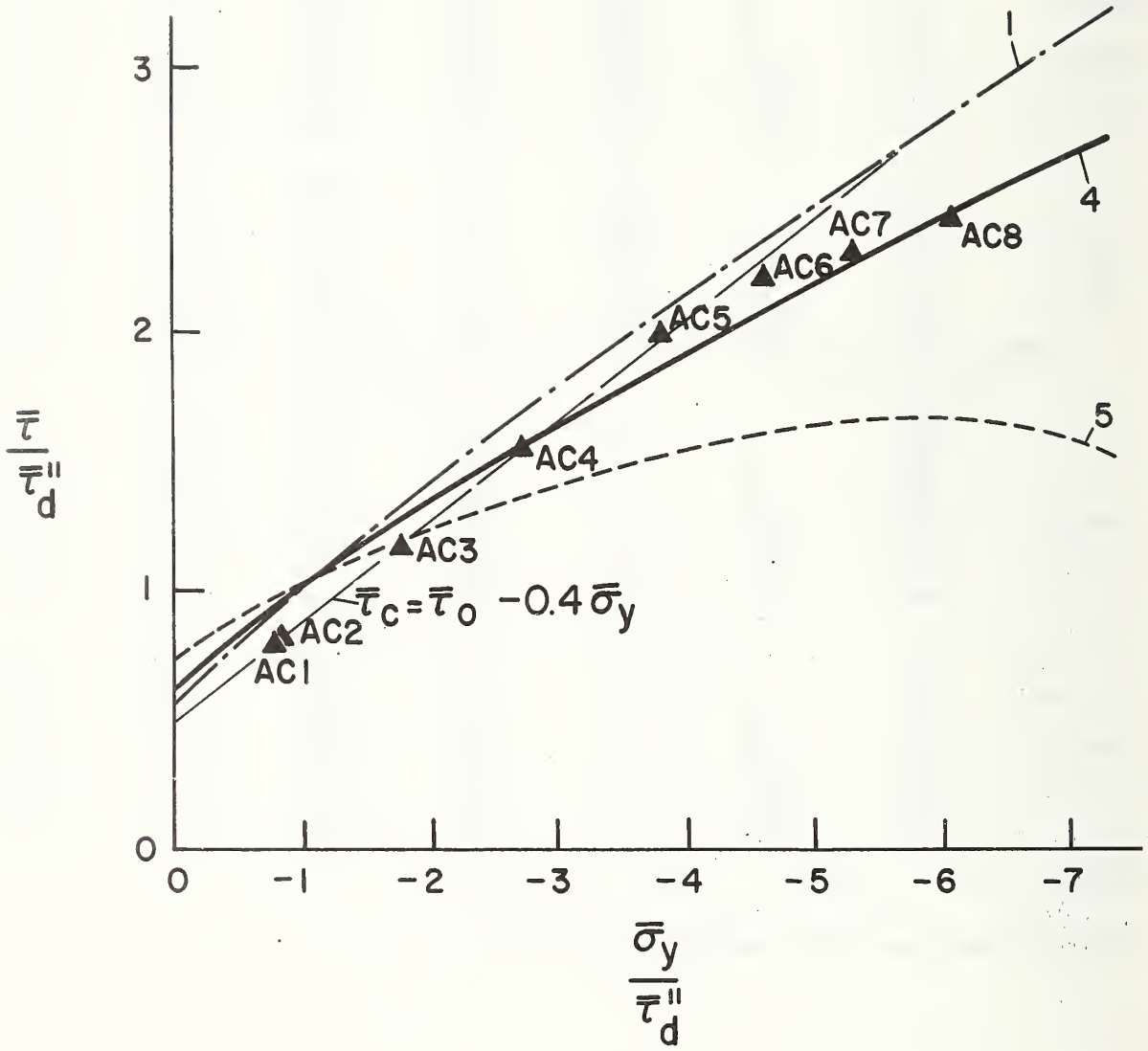

FIGURE 9 TEST SERIES AC

$$\bar{\tau}_c = \bar{\tau}_o - 0.4\ \bar{\sigma}_y \qquad \ldots\ldots(18)$$

It is observed that an extension of this line also closely predicts the failure loads of specimens AC4 and AC5. This observation suggests that in these two specimens, even though the failure had the visual appearance of splitting, this splitting failure was triggered by joint separation. This proposition is reinforced by an examination of the failure mode of specimen AC3 which exhibits characteristics of both joint separation and splitting. Specimens AC6, AC7, and AC8 plot in the vicinity of curve 4 which represents the strength envelope hypothesis for type AC masonry. However, the uncertainty in the determination of $\bar{\tau}''_d$ raises doubt about the correct position of the plotted test points for specimens AC relative to curves 1, 4, and 5.

6.2.2 Masonry Type AH

The AH test series is plotted in figure 10 together with curves 1, 3, and 5 from figure 7. Figure 5 shows the observed failure modes. For all specimens the failure mode appears to be splitting, and for the specimens subjected to a high P_v the splitting is pronounced near the loading fixtures and does not always extend through the center of the panel.

The plot of the test results shows reasonable agreement with curve 3 for the strength-envelope hypothesis. The relatively low strength of specimen AH8 appears to be attributable to failure in locations other than the center of the panel and therefore is not adequately predicted on the basis the state of stress in the center of the panel.

6.2.3 Masonry Type BH

Figure 11 shows a plot of test series BH. Figure 6 shows the failure modes of specimens BH3 and BH7 which appear to be splitting that includes the region near the center of the panel. The plot in figure 11 shows reasonable agreement with curve 2 for the strength-envelope hypothesis.

6.2.4 Masonry Type SH

Figure 12 shows a plot of SH test series. The failure mode of specimen SH5 is shown in figure 6.

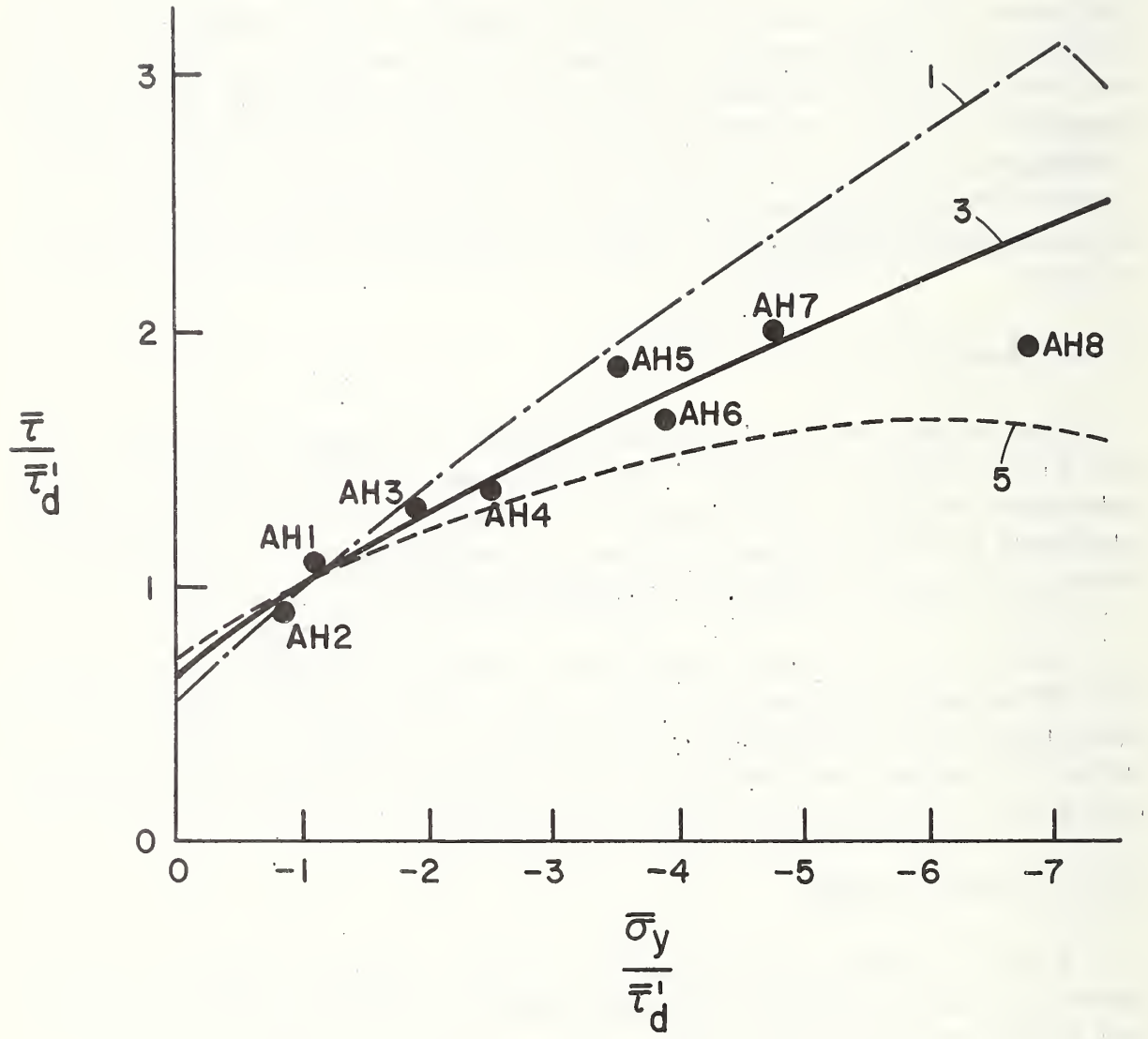

FIGURE 10 TEST SERIES AH

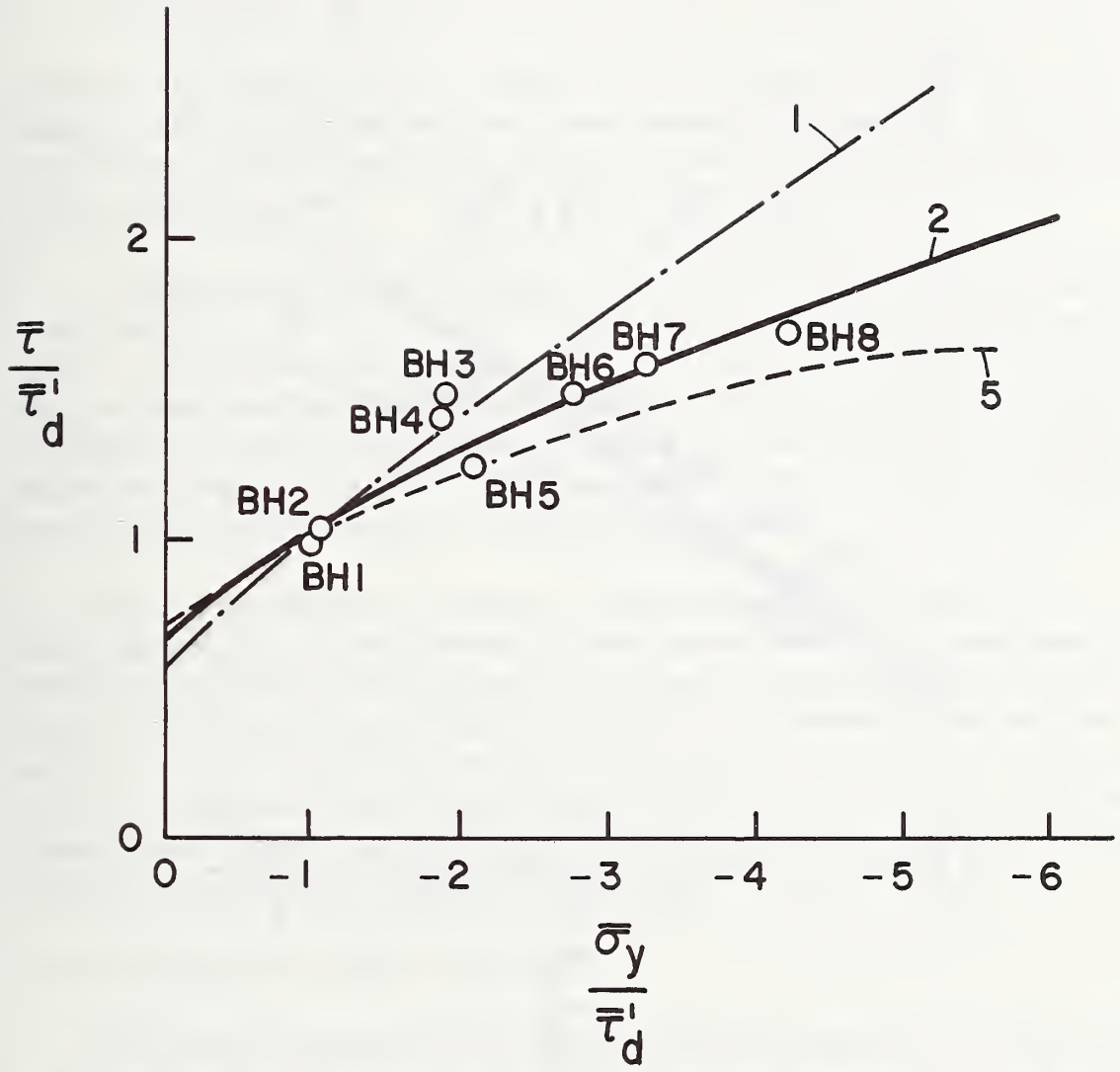

FIGURE 11 TEST SERIES BH

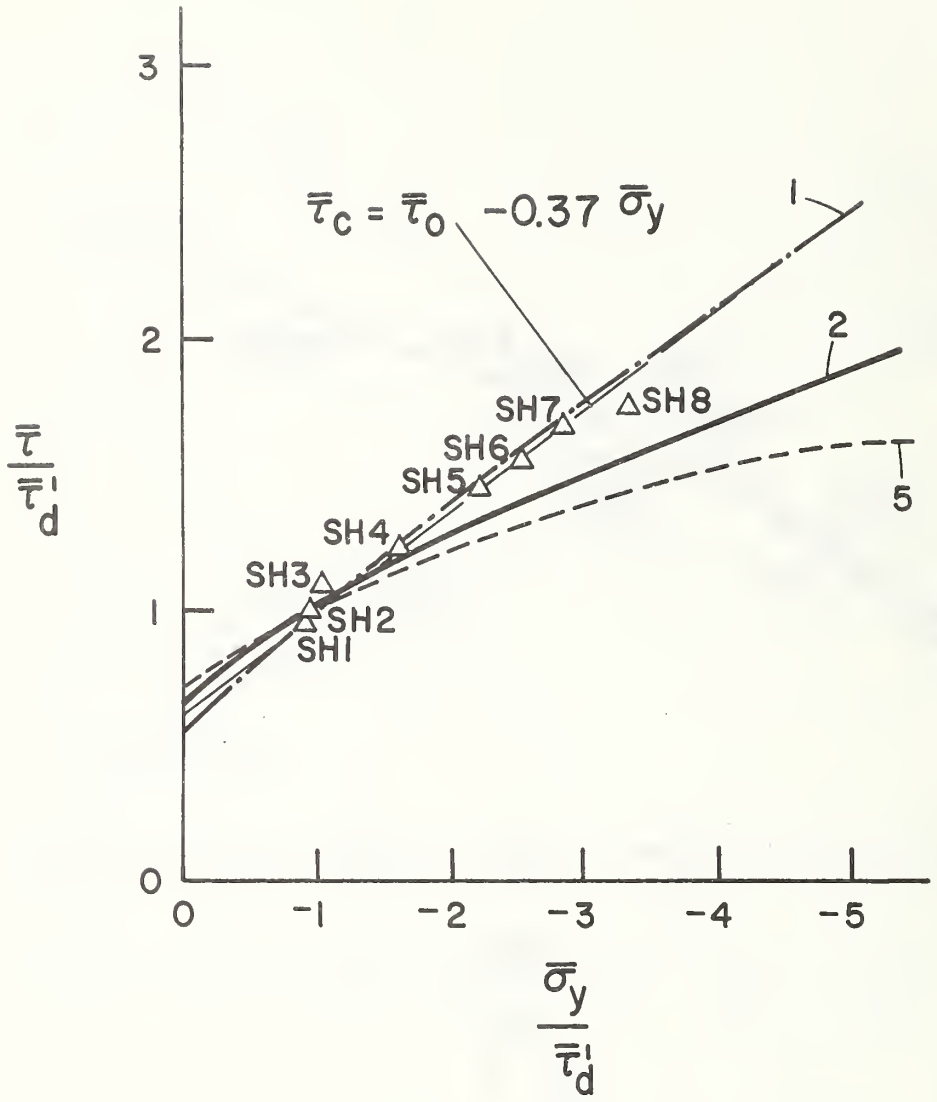

FIGURE 12 TEST SERIES SH

Tests SH1 through SH7 plot approximately on a straight line defined by the equation:

$$\bar{\tau}_c = \bar{\tau}_o - 0.37\ \bar{\sigma}_y \qquad \ldots (19)$$

Specimen SH8 falls below this line. The correlation between the tests suggest that the failure may have been caused, or triggered, by joint separation. Close examination of specimen SH5 in figure 6 reveals partial joint separation.

A contributing factor to this failure mode may have been the surface condition of the units: S units were solid, while A and B units were cored. The break in the trend of the test data evident from the relationship between specimens SH7 and SH8 suggests that at the load level of specimen SH7 there may have been a transition from joint-separation to splitting. Unfortunately SH5 (figure 6) is the only available intelligible record of a failure mode for these specimens.

Curve 1 in figure 12 provides another possible explanation for the load capacity of the SH specimens. This curve, which was calculated for failure by critical normal stress, is closely approximated by equation (18) within the range of the SH tests. It is noted, however, that the test points in this figure were arbitrarily plotted on the basis of $\bar{\tau}'_d$ rather than $\bar{\tau}''_d$. Their true position relative to curves 1, 2, and 5 is not known, since the available visual failure observation shown in figure 3 does not provide evidence of a splitting failure.

6.3 Interpretation of Test Results

The three splitting-failure hypotheses are mutually exclusive, however both splitting and joint separation could occur simultaneously in any one specimen or, for the same type of masonry, either splitting or joint separation could occur in different ranges of $\bar{\sigma}_y/\bar{\tau}'_d$.

Whether joint separation or splitting governs depends on the relative magnitude of coefficient μ in eq. (18) as well as on the resistance of the mortar joints to separation when $\bar{\sigma}_y = 0$. Coefficient μ was found to be approximately 0.4 for types AC and SH masonry. The resistance of the mortar joints to separation depends on the tensile and shear strength of the mortar joints and on the bond between mortar and masonry units. It is reasoned that f'_t, the flexural strength of a horizontal section, which depends on the tensile strength of the mortar and on the bond between the

mortar joint and the masonry unit should be related to the resistance to separation of mortar joints. Accordingly, the ratio $\bar{\tau}'_d/f'_t$ should give an indication whether the failure under load P'_d is attributable to joint separation or to splitting. These ratios are calculated below for the four types of masonry:

Type	Average $\bar{\tau}'_d$ psi	f'_t, psi	$\bar{\tau}'_d/f'_t$
AC	178	80	2.23
AH	508	360	1.41
BH	625	452	1.38
SH	740	220	3.36

NOTE: 1 psi = 6.9 kPa

The calculated ratios are substantially higher in type AC and SH masonry, which adds substance to the proposition that in these types of masonry failure under P'_d occured by joint separation. On the other hand, the ratios for AC and SH differ among themselves.

The correlation between the splitting hypotheses and the test results is examined on the basis of the AH and BH tests which failed by splitting. An examination of figures 10 and 11 shows that:

1. most test results fall below curve 1 and above curve 5;
2. the curves based on the strength envelope in figure 7 reasonably approximate the test results; and
3. for large compressive edge loads test results tend to fall below these curves.

On this basis it is concluded that the failure hypothesis based on the strength envelope in figure 8(c) provides the best predictive model for the test results. For the type of load-transfer mechanism used in these tests curves 2, 3, and 4 apply in the approximate region of $\bar{\sigma}_y/\bar{\tau}'_d > -5$. For higher compressive edge loads failure can not be predicted on the basis of the calculated state of stress in the center of the panel.

It can be shown that, for the same type of masonry, joint separation could occur below a certain compressive edge load (P_v), and splitting for higher values of P_v.

The approximate equation derived from the experimental results for joint separation is:

$$\bar{\tau}_c = \bar{\tau}_o - 0.4\ \bar{\sigma}_y \quad \ldots\ (18)$$

Curves 2-4 for the range $-1 > \bar{\sigma}_y/\bar{\tau}'_d > -5$ fall approximately between the following boundaries:

$$\bar{\tau}_c = \bar{\tau}''_o - 0.175\ \bar{\sigma}_y \quad \text{for } R = -8 \quad \ldots\ (20)$$

$$\bar{\tau}_c = \bar{\tau}''_o - 0.225\ \bar{\sigma}_y \quad \text{for } R = -16 \quad \ldots\ (21)$$

in which $\bar{\tau}''_o \geq \bar{\tau}'_o$ if failure at $\bar{\tau}'_d$ was by joint separation.

If failure at $\bar{\tau}'_d$ occurred by joint sepration the line defined by eq. (18) could intersect the linesdefined by eqs. (20 or (21) at a value of $\bar{\sigma}_y/\bar{\tau}'_d > -5$, causing the failure mode to change from joint separation to splitting. This leads to the important conclusion that the equation for joint separation should not be extrapolated beyond the range within which it is known to be valid.

6.4 Prediction of Load Capacity

If $\bar{\tau}'_d$ and f'_m are determined by test, and if the failure at $\bar{\tau}'_d$ is by diagonal splitting, $\bar{\tau}_c$ can be determined by extrapolation within the range $-1 > \bar{\sigma}_y/\bar{\tau}'_d > -5$ using curves 2, 3, or 4 or approximate eqs. (20) or (21). If $\bar{\tau}'_d$ is determined by test and failure is by joint separation, the result cannot be extrapolated without additional information on the value of μ, and on the range of $\bar{\sigma}_y/\bar{\tau}'_d$ within which joint separation failure occurs. Such information could be obtained by tests similar to those examined herein.

Whether the failure at $\bar{\tau}'_d$ was by splitting or by joint separation may be difficult to determine. Visual inspection alone may be misleading in cases similar to those discussed for specimens AC3, 4 and 5. Ratio $\bar{\tau}'_d/f'_t$ could serve as an indicator of the failure type, however the information in this paper would have to be supplemented by more test data to provide a sufficient basis for such an approach. A more reliable approach would be to provide independent information on the splitting strength envelope, coefficient μ, and the resistance to joint separation, using other test methods in addition to diagonal compressive tests. Presently used standard tests do not provide this information.

7. Summary

1. Failure under combinations of compressive diagonal and edge loads (figure 1) can occur by joint separation or splitting.

For the same type of masonry, failure may occur by joint separation under small compressive edge loads (P_v) and change to splitting above a certain level of P_v. It is therefore not advisable to extrapolate data obtained for joint separation at low levels of P_v to estimate load capacity at higher levels of P_v.

2. Those test data which provide indication of joint separation failure are in good agreement with equation (17): $\bar{\tau}_c = \bar{\tau}_o - \mu\bar{\sigma}_y$ with an approximate μ value of 0.4.

3. Where failure is caused by splitting, load capacity is reasonably predicted on the basis of the assumption that, within the range $-1 > \bar{\sigma}_y/\bar{\tau}'_d > -5$ failure originates in the center of the panel and is caused by a critical combination of principal normal stresses.

Within the same range, load capacity is overestimated by the hypothesis that failure occurs when a critical principal tensile stress is exceeded, and underestimated by the hypothesis that failure occurs at a critical extensional strain assuming a Poisson Ratio of 0.2.

8. Acknowledgement

The authors are indebted to Louis E. Cattaneo from the Center for Building Technology, National Bureau of Standards, who made available unpublished information related to Reference [4] and critically reviewed this report, and to the Brick Institute of America, the Masonry Institute of America, the National Concrete Masonry Association and the Tri-Service Building Materials Investigational Program Committee who within the framework of the "Cooperative Masonry Program" participated in the funding of an investigation of masonry shear walls which included this study.

*Departments of the Army, Navy and Airforce.

9. Bibliography

[1] ASTM Designation C67-66, "Methods of Sampling and Testing Brick", American Society for Testing and Material, Philadelphia, Pa., 1966.

[2] Blume, T. A., and Prolux, J., "Shear in Grouted Brick Masonry Wall Elements," Western States Clay Products Association, San Francisco, Cal., 1968.

[3] Frocht, M.M., "Recent Advances in Photoelasticity," Transactions ASME, Vol. 55, pp. 135-153, Sept. - Dec. 1931.

[4] Grenley, D. G. and Cattaneo, L. E., "The Effect of Edgeload on Racking Strength of Clay Masonry," Proceedings, Second International Brick Conference, Stoke on Trent, G. B., The British Ceramic Research Association, Stoke-on-Trent, ST4 7LQ, April 1970.

[5] Griffith, A. A., "The Phenomenon of Rupture and Flow in Solids," Phil. Trans. Roy. Soc., A221, 163, London 1921.

[6] Johnson, F. B. and Thompson, T. M., "Development of Diametral Testing Procedures to Provide a Measure of Strength Characteristics of Masonry Assemblages," Design Engineering and Construction of Masonry, F. B. Johnson, ed., Gulf Publishing Co., Houston, Texas 1969.

[7] Khoo, C. L. and Hendry, A. M., "A Failure Criterion for Brickwork in Axial Compression," Preprint 2b2, 3rd International Masonry Conference, Essen, Germany, 1973.

[8] Kupfer, H., Hilsdorf, H. K., and Rusch, H., "Behavior of Concrete under Biaxial Stresses," J., American Concrete Institute, Vol. 66, No. 8 August 1969.

[9] Reichard, T. W., "Creep and Drying Shrinkeage of Lightweight and Normal Weight Concrete," NBS Monograph 74, National Bureau of Standards, Washington, D. C., (1964).

[10] Sahlin, S., "Chapter D", Structural Masonry, Prentice-Hall, Inc., Clifton, N.J. 1971.

[11] ibid., "Chapter G"

[12] Timoshenko, S., "Chapter 10, pp. 459-462," Strength of Materials, Part II, 3rd Ed., Van Norstrand, N.Y., 1956.

APPENDIX

Derivation of Equations for Splitting Failure Hypotheses

A.1 General

For brevity, the symbol "~" is introduced in the following derivations to denote stresses normalized with respect to $\bar{\tau}'_d$ which is defined by eq. (6). Accordingly, the general (biaxial, in this c state of stress at the center of a square panel under diagonal and edge loading (figure 1) is described by reference to figure 3(b) as follows,

$$\tilde{\sigma}_x = -0.823\ \tilde{\tilde{\tau}} \qquad \ldots\ldots\ldots \text{(A.1)}$$

$$\tilde{\tau}_y = \tilde{\sigma}_v - 0.823\ \tilde{\tilde{\tau}} \qquad \ldots\ldots\ldots \text{(A.2)}$$

$$\tilde{\tau}_{xy} = 1.557\ \tilde{\tilde{\tau}} \qquad \ldots\ldots\ldots \text{(A.3)}$$

where $\tilde{\sigma}_x = \sigma_x/\bar{\tau}'_d$, $\tilde{\sigma}_y = \sigma_y/\bar{\tau}'_d$ and so on. Likewise, division of eqs. (3) and (4) by $\bar{\tau}'_d$ yields the corresponding equations for the non-dimensionalized principal stresses

$$\tilde{\sigma}_1 = -0.823\ \tilde{\tau} + \frac{\tilde{\sigma}_v}{2} + \sqrt{(1.556\ \tilde{\tilde{\tau}})^2 + \frac{\tilde{\sigma}_v^2}{4}} \qquad \text{(A.4)}$$

$$\tilde{\sigma}_3 = -0.823\ \tilde{\tilde{\tau}} + \frac{\tilde{\sigma}_v}{2} - \sqrt{(1.556\ \tilde{\tilde{\tau}})^2 + \frac{\tilde{\sigma}_v^2}{4}} \qquad \text{(A.5)}$$

The equation

$$\tilde{\tilde{\sigma}}_y = \tilde{\sigma}_v - \tilde{\tilde{\tau}} \qquad \ldots\ldots\ldots \text{(A.6)}$$

which follows from the definitions of nominal stresses given in Section 3, may be used to eliminate $\tilde{\sigma}_n$ from eqs. (A.4) and (A.5). The resulting equations

$$\tilde{\sigma}_1 = -0.323\ \tilde{\tilde{\tau}} + \frac{\tilde{\tilde{\sigma}}_y}{2} + \sqrt{2.67\ \tilde{\tilde{\tau}}^2 + 0.5\ \tilde{\tilde{\tau}}\tilde{\tilde{\sigma}}_y + 0.25\ \tilde{\tilde{\sigma}}_y^2} \qquad \text{(A.7)}$$

$$\tilde{\sigma}_3 = -0.323\ \tilde{\tilde{\tau}} + \frac{\tilde{\tilde{\sigma}}_y}{2} - \sqrt{2.67\ \tilde{\tilde{\tau}}^2 + 0.5\ \tilde{\tilde{\tau}}\tilde{\tilde{\sigma}}_y + 0.25\ \tilde{\tilde{\sigma}}_y^2} \qquad \text{(A.8)}$$

simplify the subsequent formulations of $\tilde{\tilde{\tau}}$ as an explicit function of $\tilde{\tilde{\sigma}}_y$.

A.2 Failure by Critical Normal Stress

According to this hypothesis, failure occurs when either σ_1 or σ_3 attains its critical stress level for a given configuration of diagonal and edge load intensities. Under the assumption that critical tensile stress is attained first, eq. (1) becomes

$$\sigma_1 = 0.734\ \bar{\tau}'_d$$

or

$$\tilde{\sigma}_1 = 0.734 \qquad \ldots\ldots \text{(A.9)}$$

The equation for the tensile failure envelope (curve 1 in figure 8) is derived by solving eq. (A.7) for $\tilde{\tilde{\tau}}$ after substituting the value of σ_1 from eq. (A.9),

$$\tilde{\tilde{\tau}} = 0.0922 - 0.1601\ \tilde{\tilde{\sigma}}_y + \sqrt{0.0256\ \tilde{\tilde{\sigma}}_y^2 - 0.3152\ \tilde{\tilde{\sigma}}_y + 0.2181} \quad \ldots \text{(A.10)}$$

The case of zero edge load ($\tilde{\sigma}_v = 0$) which should correspond to failure under diagonal load alone, is represented by the point ($\tilde{\tilde{\sigma}}_y = -1$, $\tilde{\tilde{\tau}} = 1$), as may be readily verified by substituting these values in eqs. (A.6) and (A.10). The $\tilde{\tilde{\tau}}$-axis intercept of curve 1 in figure 7 ($\tilde{\tilde{\sigma}}y = 0$, $\tilde{\tilde{\tau}} = 0.559$) calculated from equation (A.10) corresponds to the case of a positive (tensile) edge load which is equal (and opposite) to the vertical component of the diagonal load at failure, as may be ascertained from eq. (A.6). The maximum positive edge load for which eq. (A.10) is valid may be calculated by equating the expression under the radical sign to zero, solving for $\tilde{\tilde{\sigma}}_y$, substituting it back into eq. (A.10) and solving for $\tilde{\tilde{\tau}}$. The resulting values are ($\tilde{\tilde{\sigma}}_y = 0.635$, $\tilde{\tilde{\tau}} = 0.159$) which, upon substitution into eq. (A.6) yield $\tilde{\sigma}_v = 0$. This places a lower bound on curve 1 in figure 7 so that the following should hold if eq. (A.10) were to be valid,

$$\tilde{\tilde{\sigma}}_y \geq 0.635,\ \tilde{\tilde{\tau}} = 0.159 \text{ and } \tilde{\sigma}_v \geq 0.794$$

As the edge load increases in the negative sense (compression), curve 1 approaches the asymptote $\tilde{\tilde{\sigma}}_y/\tilde{\tilde{\tau}} = -3.123$ which may be verified from eq. (A.7) by setting $\tilde{g}_1 = 0$.

Noting that $\tilde{\sigma}_3$ is equal to R' defined by eq. (7), the equation for the compressive failure envelope is derived from eq. (8) after substituting R' for $\tilde{\sigma}_3$,

$$\tilde{\tilde{\tau}} = 0.1257R' - 0.1601\ \tilde{\tilde{\sigma}}_y + \sqrt{0.4050(R')^2 - 0.4294R'\ \tilde{\tilde{\sigma}}_y + 0.0256\ \tilde{\tilde{\sigma}}_y^2} \quad \ldots \text{(A.11)}$$

Curves 1(a) and 1(b) in figure 7 were constructed using R' = -8.3 and R' = -9.7 in eq. (A.11) respectively, which were typical for the test specimens at hand (Section 5.2). Depending on the value of R', one or the other of these curves together with curve 1 define the failure envelope for the critical normal stress hypothesis. Note that curve 1 and the $\tilde{\tilde{\sigma}}_y$-axis define the physical bounds within which eq. (A.11) is valid while curve 1(a) or 1(b) imposes an upper bound on eq. (A.10). These junction points (of discontinuity) delineate a state of stress at which tension and compression attain their critical values simultaneously.

A.3 Failure by Critical Combination of Normal Principal Stresses

On the basis of the idealized strength envelope depicted in figure 8(c), the bilinear relationship between $\tilde{\tilde{\sigma}}_1$ and $\tilde{\tilde{\sigma}}_3$ as prescribed by eqs. (11) and (13) describes the critical stress combination for which failure is imminent according to this hypothesis. The failure envelope corresponding to the region in the second quadrant of figure 8(c), is derived by normalizing eq. (11) as follows,

$$\tilde{\sigma}_1 = \frac{1}{R} (R' - \tilde{\sigma}_3) \qquad \ldots\ldots \text{(A.12)}$$

and combining it with eqs. (A.7) and (A.8). The resulting equation

$$[2.6742\ (R - 1)^2 - 0.1043\ (R + 1)^2]\tilde{\tilde{\tau}}^2$$

$$+ [0.5\ (R - 1)^2\ \tilde{\tilde{\sigma}}_y + 0.323\ (R + 1)^2\ \tilde{\tilde{\sigma}}_y - 0.646\ R'(R + 1)]\tilde{\tilde{\tau}}$$

$$+ [R'(R + 1)\ \tilde{\tilde{\sigma}}_y - R\tilde{\tilde{\sigma}}_y^2 - (R')^2] = 0 \qquad \ldots\ldots \text{(A.13)}$$

was used to construct the ascending portions of curves 2, 3 and 4 of figure 7, for the respective R' values of -8.3, -9.7 and -14.1, which are representative of three types of masonry used in the tests. The corresponding values of R, namely -8, -10 and -16, used in the same equation, were calculated in accordance with equation (10).

The equation for that portion of the failure envelope falling in the third quadrant of figure 8(c) is obtained by normalizing eq. (13) as follows

$$\tilde{\sigma}_1 = \tilde{\sigma}_3 - R' \qquad \ldots\ldots \text{(A.14)}$$

and combining it with eqs. (A.7) and (A.8). The resulting equation

$$\tilde{\tilde{\tau}}^2 + (0.187\ \tilde{\tilde{\sigma}}_y)\ \tilde{\tilde{\tau}} + 0.0935\ [\tilde{\tilde{\sigma}}_y^2 - (R')^2] = 0 \qquad \ldots \text{(A.15)}$$

was used to construct the descending portions of curves 2, 3 and 4 (the latter falls outside the range shown in figure 8) for the same values of R' and R as used in eq. (A.13).

A.4 Failure by Critical Extensional Strain

According to this hypothesis, failure will occur when the principal extensional strain attains a critical magnitude K. Stated mathematically,

$$\tilde{\sigma}_1 - \nu\tilde{\tilde{\sigma}}_3 = K \qquad \ldots\ldots \text{(A.16)}$$

where ν is the Poisson's ratio. The constant K = 1.21 is evaluated by substituting $\tilde{\sigma}_1 = 0.734$ and $\tilde{\sigma}_3 = -2.380$ obtained from eqs. (1) and (2) for the critical state at zero edge load together with $\nu = 0.2$ used in this study into eq. (A.16). This gives

$$\tilde{\sigma}_1 - 0.2\,\tilde{\sigma}_3 = 1.21 \qquad \ldots\ldots \text{(A.17)}$$

which, when used in combination with eqs. (A.7) and (A.8), yields the equation for the failure envelope of this hypothesis. Noting, however, the similarity of eqs. (A.17) and (A.12), the governing equation in this case may be readily obtained from eq. (A.13). From eqs. (A.12) and (A.17),

$$\frac{R'}{R} - \frac{\tilde{\sigma}_3}{R} = 1.21 + 0.2\,\tilde{\sigma}_3 \qquad \ldots\ldots \text{(A.18)}$$

which, together with eq. (10), yields R = -5 and R' = -6.05. Substitution of these values in eq. (A.13) gives

$$\tilde{\tilde{\tau}} = 0.0826 - 0.1224\,\tilde{\tilde{\sigma}}_y + \sqrt{0.3937 - 0.276\,\tilde{\tilde{\sigma}}_y - 0.0378\,\tilde{\tilde{\sigma}}_y^2} \quad \text{(A.19)}$$

or

$$\tilde{\tilde{\sigma}}_y = -2.42 - 2.3168\,\tilde{\tilde{\tau}} - \sqrt{13.177 + 14.34\,\tilde{\tilde{\tau}} - 13.553\,\tilde{\tilde{\tau}}^2} \quad \text{(A.20)}$$

Curve 5 in figure 7 was constructed using either equation. Since the bounds of this curve fall outside the quadrant of interest shown in figure 8, they need not be established.

NBS-114A (REV. 7-73)

U.S. DEPT. OF COMM BIBLIOGRAPHIC DATA SHEET	1. PUBLICATION OR REPORT NO. NBSIR 75-703	2. Gov't Accession No.	3. Recipient's Accession No.

4. TITLE AND SUBTITLE

A Failure Hypothesis for Masonry Shearwalls

5. Publication Date

6. Performing Organization Code 461.01

7. AUTHOR(S) Felix Y. Yokel and S. George Fattal

8. Performing Organ. Report No. NBSIR 75-703

9. PERFORMING ORGANIZATION NAME AND ADDRESS

NATIONAL BUREAU OF STANDARDS
DEPARTMENT OF COMMERCE
WASHINGTON, D.C. 20234

10. Project/Task/Work Unit No. 4615364

11. Contract/Grant No.

12. Sponsoring Organization Name and Complete Address *(Street, City, State, ZIP)*

National Bureau of Standards
Department of Commerce
Washington, D. C. 20234

13. Type of Report & Period Covered

14. Sponsoring Agency Code

15. SUPPLEMENTARY NOTES

16. ABSTRACT *(A 200-word or less factual summary of most significant information. If document includes a significant bibliography or literature survey, mention it here.)*

Various failure hypotheses for wall panels subjected simultaneously to diagonal compressive load and to vertical compressive edgeload are compared with the results of thirty-two tests on four types of brick masonry walls which were published elsewhere. It is concluded that failure can occur by joint separation or by splitting. A failure hypothesis is advanced which is shown to be in good agreement with the test results examined.

17. KEY WORDS *(six to twelve entries; alphabetical order; capitalize only the first letter of the first key word unless a proper name; separated by semicolons)* Brick; failure; failure theories; masonry; shear walls; shear strength; shear test; stresses; stress distribution; structural engineering.

18. AVAILABILITY

[x] Unlimited

[ ] For Official Distribution. Do Not Release to NTIS

[ ] Order From Sup. of Doc., U.S. Government Printing Office Washington, D.C. 20402, SD Cat. No. C13

[x] Order From National Technical Information Service (NTIS) Springfield, Virginia 22151

19. SECURITY CLASS (THIS REPORT)	21. NO. OF PAGES
UNCLASSIFIED	38
20. SECURITY CLASS (THIS PAGE)	22. Price
UNCLASSIFIED	$3.75

USCOMM-DC 29042-P74